Biomed Microdevices (2011) 13:361–373
DOI 10.1007/s10544-010-9505-3

Highly-compliant, microcable neuroelectrodes fabricated from thin-film gold and PDMS

Maxine A. McClain · Isaac P. Clements · Richard H. Shafer · Ravi V. Bellamkonda · Michelle C. LaPlaca · Mark G. Allen

Published online: 15 January 2011

Abstract Bio-electrodes have traditionally been made of materials such as metal and silicon that are much stiffer than the tissue from which they record or stimulate. This difference in mechanical compliance can cause incomplete or ineffective contact with the tissue. The electrode stiffness has also been hypothesized to cause chronic low-grade injury and scar-tissue encapsulation, reducing stimulation and recording efficiency. As an initial step to resolve these issues with electrode performance, we have developed and characterized electrically-functional, low-Young's modulus, microcable-shaped neuroelectrodes and demonstrated electrophysiological recording functionality. The microcable geometry gives the electrodes a similar footprint to traditional wire and microwire neuroelectrodes, while reducing the difference in Young's modulus from nervous tissue by orders of magnitude. The electrodes are composed of PDMS and thin-film gold, affording them a high-level of compliance that is well suited for *in vivo* applications. The composite Young's modulus of the electrode was experimentally determined to be 1.81± 0.01 MPa. By incorporating a high-tear-strength silicone, Sylgard 186, the load at failure was increased by 92%, relative to that of the commonly used Sylgard 184. The microcable electrodes were also electromechanically tested, with measurable conductivity (220 kΩ) at an average 8% strain (n=2) after the application of 200% strain. Electrophysiological recording is demonstrated by wrapping the electrode around a peripheral nerve, utilizing the compliance and string-like profile of the electrode for effective recording in nerve tissue.

Keywords Microelectrode · Neuroelectrode · Neural electrode · PDMS · Elastomer · Elastomeric · Thin-film gold · Brain-machine interface · DBS · Neural prosthesis

1 Introduction

Biomedical MEMS for *in vivo* or *in vitro* applications utilize small feature sizes to unobtrusively monitor biological processes and effectively interface with cellular-level targets (Takei et al. 2009; Wu et al. 2005). Silicone is a low Young's modulus polymer with extensive applications in implantable devices (Jackson et al. 2009; Wasikiewicz et al. 2008; Williams 2008). Sylgard 184, a polydimethyl siloxane (PDMS) formulation of silicone commonly used in bioMEMS devices, has an elastic modulus lower than other polymers commonly used in microelectronics (Table 1). (Sylgard 184 is regarded as non-toxic, but is not medical grade and as such is used as a cost-effective solution in many pre-clinical settings. Comparable medical grade silicones are Med-6215 and Med-6210 (Nusil; Carpinteria, CA)). If the implant impedes or opposes the movement and growth of the surrounding tissue, it can cause injury and scarring (Chiono et al. 2009). A reduction in the difference in stiffness or an improvement in the mechanical coupling between the implant and surrounding tissue results in reduced inflammation (Biran et al. 2007;

Electronic supplementary material The online version of this article (doi:10.1007/s10544-010-9505-3) contains supplementary material, which is available to authorized users.

M. A. McClain (✉) · R. H. Shafer · M. G. Allen
Electrical and Computer Engineering,
Georgia Institute of Technology,
Atlanta, GA 30332, USA
e-mail: Maxine.mcclain@gatech.edu

I. P. Clements · R. V. Bellamkonda · M. C. LaPlaca
Biomedical Engineering,
Georgia Institute of Technology/Emory University,
Atlanta, GA 30332, USA

Table 1 Young's modulus values for potential electrode polymer substrates and neural tissues. References PDMS: (Sun et al. 2004), Parylene C (Pornsin-Sirirak et al. 2001) SU-8 (Al-Halhouji et al. 2008); Kapton (DuPont 2009); Brain (Green et al. 2008), Peripheral nerve (Borschel et al. 2003)

Polymer	Young's modulus
PDMS	~1 MPa
Parylene C	4.5 GPa
SU-8	3.5–7.5 GPa
Polyimide (Kapton ®)	2.4–3.2 GPa
Brain	3.15 kPa
Peripheral nerve	576±160 kPa

Rousche et al. 2001; Seymour and Kipke 2007; Stice et al. 2007; Young 1989). Although the Young's modulus range of PDMS is higher than peripheral and brain tissues, it is several orders of magnitude lower than several alternative materials (Table 1). Additionally PDMS-based bioMEMS can be molded for a specific surface topography effectively and efficiently on the microscale (Xia and Whitesides 1998).

The prior literature on PDMS-based electronics includes structures intended to be either compliant or both compliant and stretchable (Meacham et al. 2008; Yu et al. 2007). Devices with PDMS as the primary substrate are intrinsically elastomeric. Elastomeric electronics are frequently comprised of an elastomer with embedded conductive particulates, such as graphite, carbon nanotubes, or metal ions (Maiti et al. 2008; Mark 2006; Rosset et al. 2009; Someya et al. 2004). Using bulk electrically conductive elastomers in micropatterned devices presents challenges in patterning conductive material precisely with selectively insulated and exposed regions. Thin-film gold metallization of PDMS addresses these concerns. Gold is frequently patterned in microfabricated devices and PDMS can be patterned with metal using a subset of standard process techniques (Yu et al. 2007). Gold has relatively soft and ductile mechanical properties, which are advantageous for use in elastomer electronics (Weast 1979). Additionally, gold does not form a surface oxide, making it suitable for electrode recording sites (Cogan 2008). PDMS shape and topography can be controlled by several methods, including photosensitive polymerization, laser ablation, reactive ion etching (RIE), and micromolding (Garra et al. 2002; Graubner et al. 2002; Sayah et al. 2007; Sia and Whitesides 2003).

2 Electrode design

The electrodes presented here, with a microcable geometry, are intended as a demonstration of small-footprint conformal electrodes. Highly conformal electrodes of PDMS have been previously demonstrated in several instances in a sheet-like array format, and shank style electrodes are available for routine intracortical use, have been made of wire, silicon and polymers such as polyimide and parylene C (Biran et al. 2007; Graz et al. 2009; Lacour et al. 2004; Li and Suo 2006; Rousche et al. 2001; Seymour and Kipke 2007). The electrodes presented here are made of a combination of PDMS and thin film gold, which affords them a low compliance relative to other shank-style neural electrodes, while maintaining a small-footprint with the shank profile. The demonstration of electrode function, with the recording of a compound action potential from the sciatic nerve in a rat, is intended to show that the electrodes can wrap around small features (diameter~1 mm), demonstrating a high level of conformability as shown by the schematic in Fig. 1. The cross-section of the electrode is 80×200 μm. Although many of the initial studies of gold and thin-film PDMS have used a relatively thick 1 mm substrate (Graz et al. 2009; Lacour et al. 2004; Li and Suo 2006), the desirability of a thinner substrate has been recognized with the publication of sheet-like arrays on 75 μm thick PDMS (Adrega and Lacour 2010). These thinner sheets approach the thickness of commercially available silicon electrode arrays (NeuroNexus Technologies; Ann Arbor, MI) The microcable electrodes demonstrated here could be made narrower, but in this prototype, the 100 μm wide gold leads are patterned with a

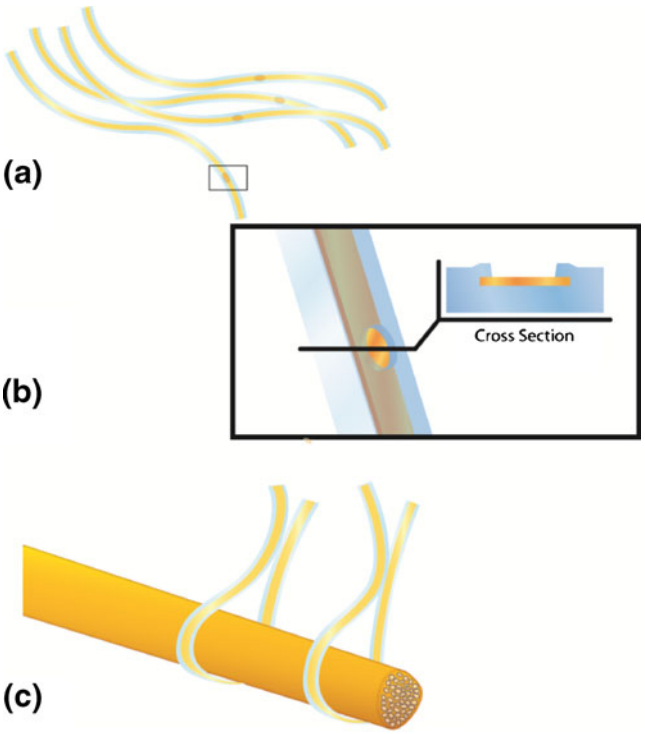

Fig. 1 (**a**) A schematic of flexible, string-like electrodes arrays is shown above, with (**b**) a cross-section of the recording site. (**c**) The electrodes are designed to be highly conformal and have a small footprint to facilitate contact with small or high-curvature anatomical features such peripheral nerves

stencil, which is easily aligned by hand on the 200 μm wide substrate. The small footprint of the microcable profile, when used in an array format, improves the conformability to irregular surfaces compared to an electrode array patterned on a planar sheet. By creating a web or net-like electrode array, the electrodes can be clustered together or spread apart as needed and the conformation of one microcable does not impede the conformation of the neighboring cables. Conversely, for a sheet-like substrate, the electrode spacing is fixed and the surrounding features can limit or prevent contact between the device and target surface. Additionally, the open construction of the microcable array makes it "breathable," which is desirable for sensors and electronics placed on the skin for functional prosthetics (Lacour et al. 2004). A second benefit of compliance is that decreasing the difference in mechanical properties between the implant and the surrounding soft tissue has been shown to reduce the level of inflammation at the implant site (Rousche et al. 2001). For comparative purposes, the Young's moduli for brain and peripheral nerve are 3.15 kPa to 576 kPa, respectively (Borschel et al. 2003; Graz et al. 2009).

The PDMS substrate, although it was chosen for its low Young's modulus, is intrinsically elastomeric. Because the electrodes will be prone to elastic deformation during handling, the integrity of the electrical connection under strain must also be considered. The use of very thin-film metal for the conductive part of the electrode allows the electrode to be stretched out of shape, repeatedly, without a permanent loss of conductivity upon release. (It also minimizes the increase in bending stiffness found with a thicker metallic film.) Because of its elastomeric properties, the electrode may be stretched during handling and placement or during bodily movement after implantation. The movement of the implant within the body may vary from tens of microns, as described in a rodent model of cortical electrode implants (He and Bellamkonda 2008), to levels significant enough that the electrode must be designed to minimize strain coupling to the extent possible, as in the case of implant locations in the peripheral nervous system, (Scheiner et al. 1994, 2008). To realistically estimate the percent strain in an implant environment, the electrode length, tension and site of implantation must be considered with respect to the geometry (Kumar et al. 2006). As a preliminary and general demonstration of these elastomeric microcable electrodes, we are testing the electrode tolerance for deformation during handling and implantation.

The technique used to fabricate the microelectrodes described here is a derivative of micromolding technology. The advantages of micromolding include the reusable mold and bench-top fabrication. The use of spin-cast micromolding (SCμM) is simpler and easier to implement than RIE etching or laser (Garra et al. 2002; Graubner et al. 2002; Sayah et al. 2007; Sia and Whitesides 2003). Spin-casting techniques are also gentle in the sense that no high-energy ablation mechanism or harsh chemicals are required, which can be a concern when dealing with polymers and very thin-film metals. The spin-casting technique, which creates through-hole features in a PDMS sheet, was initially developed to create patterned membranes for tissue engineering applications (Ostuni et al. 2000). However, PDMS is an effective insulator that can be difficult to etch, especially for microscale patterns, so the SCμM process has also been applied to patterning insulation for microscale, electrically-active devices (McClain et al. 2009; Nam et al. 2006). The through-holes created by SCμM can be used to create simple vias, as well as microcables and web-like sheets which can be used in electrically-functional structures (Fig. 2) (McClain et al. 2009). The microcable length can be tailored to the application as it is determined by the length of the trough-like features in the mold (Fig. 2(a)-(b)). The posts on the mold retain a PDMS, sheet-like frame around the microcable array for packaging purposes.

The packaging was designed for versatility in testing and to demonstrate potential electrode configurations. The mechanical testing required a resistance measurement across the length of the microcable, so the length of the microcable includes a contact pad at each end. Handling the microcables was facilitated by framing them within a larger PDMS sheet. The microcables were fabricated in a quad-array to demonstrate the packaging configuration available for applications requiring an electrode array format. The individual or pairs of microcables were cut from the array as needed for testing. The microcables (Fig. 2(b), (d)) were designed to span two millimeters before the gold trace continues onto the contiguous PDMS frame. The two millimeter length was chosen because it was long enough for both mechanical and electrophysiological testing.

3 Methods

3.1 Microfabrication

This fabrication process and its rationale have been previously described in more detail (McClain et al. 2009). The steps are briefly recounted here, with modifications noted. The mold for the array was photolithographically patterned with SU-8 photoepoxy according to the manufacturer datasheet (Microchem; Newton, MA). The photomasks were emulsion-printed mylar sheets (Fine Line Imaging; Colorado Springs, CO). A test-grade silicon wafer was coated with a 2 μm layer of SU-8 2002, flood exposed and hard baked. A second 80 μm thick layer of SU-8 2025

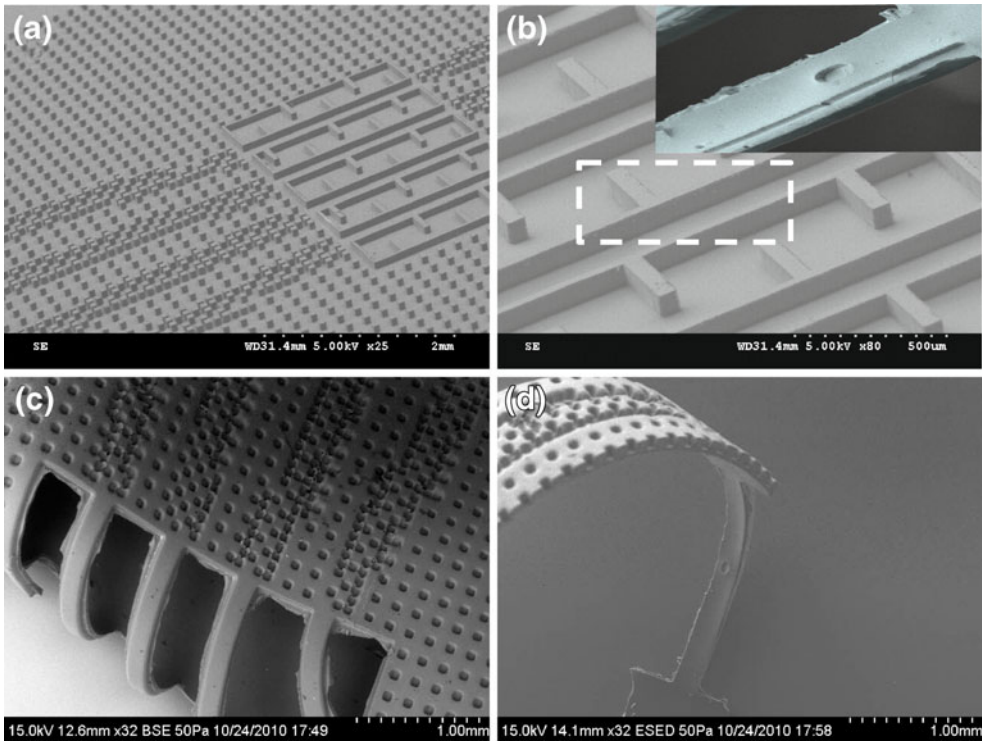

Fig. 2 (**a**) The SU-8 mold shows the straight troughs that define the microcables and the posts that act to retain PDMS in the spin-casting. The mold was designed to create a microcable array within a larger, framing, PDMS membrane. The variations in post spacing facilitated alignment of the metallization stencil. (**b**) A close up view of the microcable troughs with a released microcable shown top right (inset). The elliptical feature in the microcable is an electrode recording site (inset). The side-tabs on either side of the mold's microcable defining walls were included to help anchor the walls to the substrate during SU-8 processing. (**c**) A microcable array is shown from the underside after release. The top surface is smooth. The cross-sectional thickness of the post-imprinted sheet is 100 μm. The post height is 80 μm, and the PDMS thickness above the post height is 20 μm thick. (**d**) A microcable that has been cut apart from the array has been folded to show both the underside and the top surface

was spun-cast, patterned, and developed as the mold substrate. The heights of the mold features were confirmed with an optical micrometer (Quadra-Chek 200; Metronics; Bedford, NH).

The release layer, 20% v/w dextran (Sigma; St Louis MO) in DI water, was spun on the mold after a 30 s oxygen plasma treatment (Plasma Cleaner; Yield Engineering Systems, Inc.; Livermore, CA). The dextran was applied twice, spun 40 s at 800 rpm, and each layer was air dried before the next application. Sylgard 184 and Sylgard 186 PDMS were mixed together in a 1:1 wt ratio and spun onto the mold at 4,000 rpm for 30 s. The thickness of the spun cast silicone was 85 μm in the microcable region.

The gold for the leads was thermally deposited. The stencils to pattern the leads were made of 125 μm thick brass sheets, cut using an IR laser (Resonetics; Nashua, NH). The stencils were aligned to the substrate by hand, under a stereomicroscope, and taped into place. Prior to deposition, the wafer was oxygen plasma treated for 60 s. A PVD 75 filament evaporator (Kurt J Lesker; Clairton, PA) was used for the thermal deposition of a 5 nm chrome adhesion layer and a 30 nm gold layer. The deposition was done at 10^{-5} Torr. After deposition, the stencils were removed by hand.

The photoresist posts used to pattern a sacrificial mold for the recording sites were patterned with NR9-8000 photoresist (Futurrex; Franklin, NJ), spun 30 μm thick, pre- and post-exposure baked in an oven at 85°C, for 5 min, patterned with an exposure dose of 850 mJ, and developed with RD-6 developer (Futurrex). The bond pads on either end of the microcables (rectangles 2×4 mm) were protected with Riston dry film resist (DuPont; Wilmington, DE). Rectangular pieces of resist (~ 5 mm x 1 cm) were cut to cover the row of bond pads at each end of the array, and the contact side of the protective cellophane backing was removed prior to application. The pieces were pressed in place over the bond pads by hand and soft-baked on the hotplate to improve adhesion (80°C, 5 m). The PDMS was then spun-cast on the substrate (4,000 rpm, 8 min; cured at 100°C for 10 min.) Immediately after the PDMS was spun-cast, the top layer of cellophane of the Riston was removed, leaving the dry film resist exposed. After curing the PDMS (100°C, 10 m, then overnight at RT), the NR9-8000 photoresist at the recording sites was

removed with acetone, leaving the metal exposed at the recording site. The Riston dry film resist was dissolved with Riston developer (DuPont). The array was then released in a water bath to dissolve the dextran, and the array was pulled off the mold with a pair of tweezers.

3.2 Mechanical testing

Tensile tests were performed on Sylgard 184 and 184/186 samples to characterize the tensile strength of the substrate prior to the fabrication of the microcable electrodes (n=3/group). The tests were conducted using distance and rate-controlled millimeter and sub-millimeter displacement (Bose Electroforce 3100 test instrument, Bose; Eden Prairie, MN). Individual PDMS microcables were mounted on paper frames, which were then coupled to the force sensor (1.0 N Interface Advanced Force and Torque Measurement; Scottsdale, AZ), mounted in-line with the displacement actuator. After the sample was mounted, the sides of the paper frame were cut so that only the tensile properties of the microcable were measured. Each microcable was tested with a monotonically increasing displacement to the point of failure (0.1 mm/s). The paper frame dimensions were measured for each sample to accurately calculate the strain rate per sample (7.8%–10% s^{-1}) and strain at failure.

The Young's modulus calculations were done on the stress–strain curve of a separate set of samples (n=3/group) that was strained from zero to ten percent. The composite Young's modulus of the electrode microcables was obtained over the same strain conditions. The microcable electrodes were tested at ten and forty percent strain to assess the tensile modulus of the electrodes and to determine if cracking of the gold film from increased strain levels would measurably reduce the modulus as (Begley and Bart-Smith 2005). The strains were applied and the resulting tensile force was concurrently recorded five times to monitor the stability of the stress–strain relation under a short sequence of cycles.

3.3 Electromechanical response to strain

Fatigue testing was performed using the Bose Electroforce 3100 test instrument (n=2 pairs of microcable arrays). The resistance was recorded during the strain with a maximum resistance measurement of 110kohm. Resistances above 110 kΩ were considered to be effectively open circuits. The electrodes were measured in pairs to increase the strain over which the resistance was measurable (parallel resistance behavior was verified, data not shown). The strain was applied as a linear-slope, cyclic displacement (80% strain s^{-1}). Because of the large number of cycles in the test, the strain was set at approximately an order of magnitude higher rate than used in the mechanical characterization. The microcable samples were mounted onto a frame with a thin layer of silicone adhesive so that only the microcable region received the applied strain. The 3D printed frame (Eden 250 3D Printer; Objet; Billerica MA) was designed with flexible elbows to isolate the testing area and provide a mechanically stable platform for the electrical connections. The electrical resistance was measured with a resistance-tracking program created using SignalExpress (National Instruments; Austin, TX) that measured the resistance, from 0–110 kΩ, as a function of time. The resistance measurement was done after the first five cycles, and after 1,000 and 5,000 cycles of applied strain.

3.4 Electrophysiological measurements

Compound nerve action potentials were recorded from the sciatic nerve of an adult Sprague–Dawley rat to assess the capability of the microcable electrodes to record electrophysiological signals (Clements et al. 2009). The rat was deeply anesthetized with 5% isoflurane gas (in O_2), and a skin incision was made along the femoral axis. The underlying thigh muscles were delineated with a blunt probe to expose the sciatic nerve, which was freed from overlying connective tissue. The microcable electrodes were pulled under and around the nerve with a pair of forceps, and the area was coated with mineral oil warmed to 37°C. Three microcable electrodes were wrapped around the nerve. A double electrode array had a separation of 1 mm. A third microcable electrode was placed on the nerve separately, separated from the double array by approximately one cm. Next, a portion of the posterior tibial nerve branch, located near the ankle, was exposed, and attached to a pair of stainless steel bipolar hook electrodes. This distally positioned pair of electrodes was attached to a stimulator (Model S88, Grass Technologies) and stimulus isolation unit (Model SIU5B, Grass), which were used to stimulate the nerve with 100 μs square pulses of variable amplitude, applied at a rate of 1 Hz. The ground electrode (a coiled wire) was placed approximately five cm from the recording electrodes. The experiment was conducted measuring the differential of the evoked action potential between the three electrodes on one animal.

Evoked compound nerve action potentials were recorded upstream from the microcable PDMS electrodes and amplified (G=1,000), band-pass filtered (300-5,000 Hz, Model 1700, A-M Systems), and digitally sampled, (25 kS/s, Multichannel Systems DAQ card.) The recordings were averaged up to 128 times, using a trigger signal provided by the stimulator. The recording set-up was designed for differential recording between two electrodes. The microcables were either divided into pairs or isolated into single electrodes so that inter-electrode spacing could be varied

for the differential measurements. The *in vivo* experiments were done using an IACUC approved protocol.

4 Results

4.1 Microfabrication

The devices were created using spin-casting of PDMS on a mold of micro-topographical features. The topographical features have two functions: 1) forming through-holes or borders in the PDMS and 2) retaining material between the mold features during the spin-casting, with the amount of material retained being a function of the feature geometry and spacing. Photoresist posts create the through-holes that form the electrode recording sites, while the SU-8 walls in the mold create the microcable profiles. The material-retaining property determines the thickness of both the microcable electrode substrate and the PDMS film that connects the microcable electrodes and facilitates electrical packaging. The SU-8 posts do not form full through-holes in the connecting PDMS sheet, in this process, although the fabrication process could be adjusted to do so, if desired. The pattern of the substrate thickness is visible on the underside of a quad-array (Fig. 2(c)-(d)). The microcables are 85 μm thick, including the insulation layer, which is approximately 5 μm. The connecting PDMS sheet in the packaging region is thicker, approximately 100 μm, with a 20 μm thick membrane on top of the thicker grid- or net-like sheet, which is equal to the mold height, 80 μm.

The straight microcables are shown after release in Fig. 3(a)-(c). The microcable thickness was 80 μm for the bottom PDMS substrate and 5-6 μm for the top insulating PDMS layer. The elliptically shaped recording site was 100 μm x 50 μm. The arrays were fabricated with the following changes to the published procedure (McClain et al. 2009): 1) The substrate thickness was increased (80 μm) to improve the tensile strength of the microcables. 2) The height of the features on the SU-8 mold features was increased for a thicker microcable substrate and the spacing between the posts was increased to accommodate the shorter spin time and thicker layer of PDMS. The PDMS polymer was changed from Sylgard 184 to a mix of Sylgard 184/186 in a 1:1 wt ratio. The Sylgard 186 has a higher tensile strength and was added to improve the durability of the microcable arrays without compromising the ability to spincast the substrate into a smooth film. Sylgard 186 was not used exclusively because it does not spin-cast into a smooth film without the addition of a solvent-based diluent. The combination of Sylgard 184 and 186 was found to improve the strength of the substrate without changing the Young's modulus (Table 2).

4.2 Mechanical testing

The PDMS microcables without gold were used to determine the load and strain at failure as well as the Young's modulus of the substrate (Table 2). The load at failure was significantly increased (n=3; 1-way Anova, 95% confidence interval) while the strain at failure showed an upward trend that was not statistically different. The microcable electrodes, with gold were approximately two and half times stiffer than the unmetallized samples. (The effect of the 5 μm insulating layer was included in the thickness calculations but was otherwise assumed negligible). The microcables patterned with gold were tested at two strain ranges (0–10% and 0–40%) to measure the effect of increasing the crack density on the Young's modulus of the sample, which was calculated from the 0–10% strain region of both sample sets (Table 3). This is confirmed because modulus of the microcables after 40% strain is lower than the modulus after 10% strain, while unmetallized samples did not show a change in modulus after 40% strain. Because the calculation for the Young's modulus of PDMS and gold considers a continuous gold film it is expected to give a higher value than the values experimentally obtained from samples with cracks in the gold film. As seen in Fig. 4, some cracks are present in the film after the device was released, due to handling and packaging of the array. The crack morphology is shown for a sample that has been exposed to minimal strain (from being released from the mold) and then 2.5 and 10% strain. The morphology of

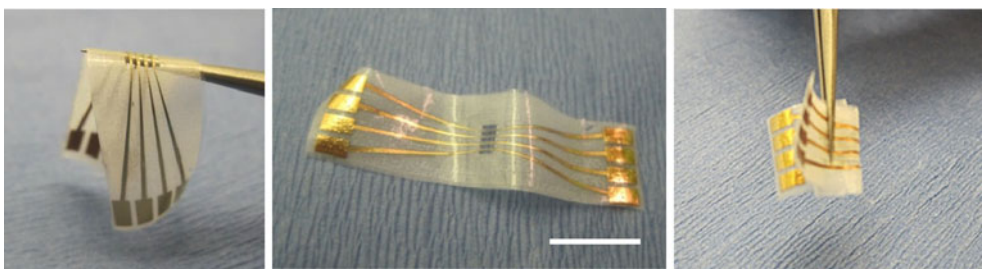

Fig. 3 The device is shown in several configurations to highlight the flexibility and conformability of the array. The design shown here was chosen for ease of use in electrical resistance monitoring both during process development and during cyclic strain tests. The design is adaptable to a shank-like profile by physically cutting the array at the end of the window defining the microcables. Scale bar: 1 cm

Table 2 Mechanical properties of the microcable substrates (n:3 for failure; n:4 for Young's modulus). The stress strain curves are provided in the supplementary data (S1-2)

Sample	Avg strain at failure (n=3)	Avg load at failure (n=3)	Young's modulus (n=4)
Sylgard 184	242% SD 6%	4.0 MPa SD: 0.38	0.72 MPa SD: 0.08 MPa
Sylgard 184/186	308% SD 16%	7.68 MPa SD: 0.29	0.69 MPa SD: 0.18 MPa

the cracks changes from a shear or diagonal orientation to one that is more orthogonal with the direction of applied strain.

The composite Young's modulus was used to compare the theoretical bending stiffness (i.e. the product of the Young's modulus and second moment of inertia of the microcable electrodes to that of the expected values of silicon or polyimide electrodes (Young 1989). The dimensions of the silicon and polyimide electrodes were obtained from the literature. The cross-sectional dimensions used for the calculations were 15×80 μm for silicon (NeuroNexus Technologies) and 30×80 μm for polyimide (Rousche et al. 2001). The PDMS microcable electrodes were 85×200 μm. The Young's moduli used in the calculations for silicon, polyimide, gold and Sylgard 184/186 were 200 GPa (Subbaroyan and Kipke 2005), 2.4 GPa (DuPont 2009), 43 GPa (Greer et al. 2006), 0.69 MPa (reported above), respectively. The effect of the gold in the silicon and polyimide calculations was not included for simplicity. The inertia was calculated using Eq. 1 and the equations for the bending stiffness of a composite beam (Eqs. 2 and 3) were used to calculate the expected bending stiffness of the microcable, modeled as a bilayer beam of composed of 85 μm of 184/186 Sylgard and 30 nm of gold (Young 1989). The variables are defined as follows: I: second moment of inertia, E: Young's modulus, w: width, t: thickness. The subscripts a and b refer to the gold and Sylgard in the bilayer beam and EI_{eq} refers to the equivalent bending stiffness.

$$I = \frac{wt^3}{12} \tag{1}$$

$$K = 4 + 6\left(\frac{t_a}{t_b}\right)^2 + \left(\frac{E_a}{E_b}\right)\left(\frac{t_a}{t_b}\right)^3 + \left(\frac{E_b}{E_a}\right)\left(\frac{t_b}{t_a}\right) \tag{2}$$

Table 3 Mechanical properties of microcable electrodes. The stress strain curves are provided in the supplementary data (S3)

(n=3)	Young's modulus after 10% strain	Young's modulus after 40% strain
Microcable electrode	1.81 MPa, SD: 12 kPa	1.62 MPa SD: 8.7 kPa

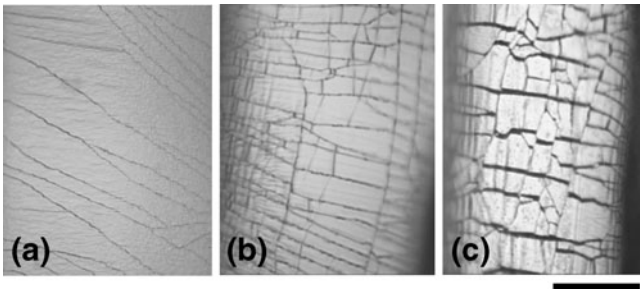

Fig. 4 The gold film is shown after the microcable electrodes have been released, from left to right, at 0, 2.5 and 10% strain. The cracks in the zero strain view are visible, with a generally diagonal orientation. The crack density increases with applied strain, as shown at 2.5 and 10%. The microcable is conductive at 2.5% strain because even though the film is cracked, there is still a conductive path. At 10% strain, the microcable is not conductive and the gold islands are visibly separated. The scale bar is 50 μm

$$EI_{eq} = K\left(\frac{wt_b^3 t_a E_a E_b}{12(t_a E_a + t_b E_b)}\right) \tag{3}$$

The calculations for the real and calculate value of the microcable and the calculated values for the silicon and polyimide electrodes are given in Table 4.

4.3 Electromechanical response to strain

The fatigue profile of the electrodes was investigated in a preliminary manner with the 200% strain tests. An example of the strain profile with the resistance measurement is shown in Fig. 5(a). After five cycles of strain, the strain-resistance profile showed a measurable resistance at 7% and 9% strain for the two microcable pairs and less than a 2% variation in the baseline resistance (Data table available in supplementary documents). The strain-resistance profile of the two samples has been overlaid for comparison in Fig. 5(b). A decrease in the range of strain with measurable conductivity and increase in the baseline resistance is found both at 1,000 and 5,000 cycles (Fig. 5(c)-(d)). The value was taken from the average resistance variation within three sequentially applied strains after a given cycle number was reached.

Table 4 The theoretical bending stiffness (EI) for the microcable electrodes is compared with the calculated value for a bilayer PDMS: gold beam and with estimated values for polyimide and silicon electrodes based on the dimensions provided in the literature

Shank-style electrodes of varying substrate materials	Theoretical bending stiffness (MPa·m^4)
PDMS microcable electrode	$1.9 \cdot 10^{-11}$
PDMS microcable electrode, expected value	$2.7 \cdot 10^{-11}$
Polyimide electrode	$4.3 \cdot 10^{-10}$
Silicon electrode	$4.5 \cdot 10^{-9}$

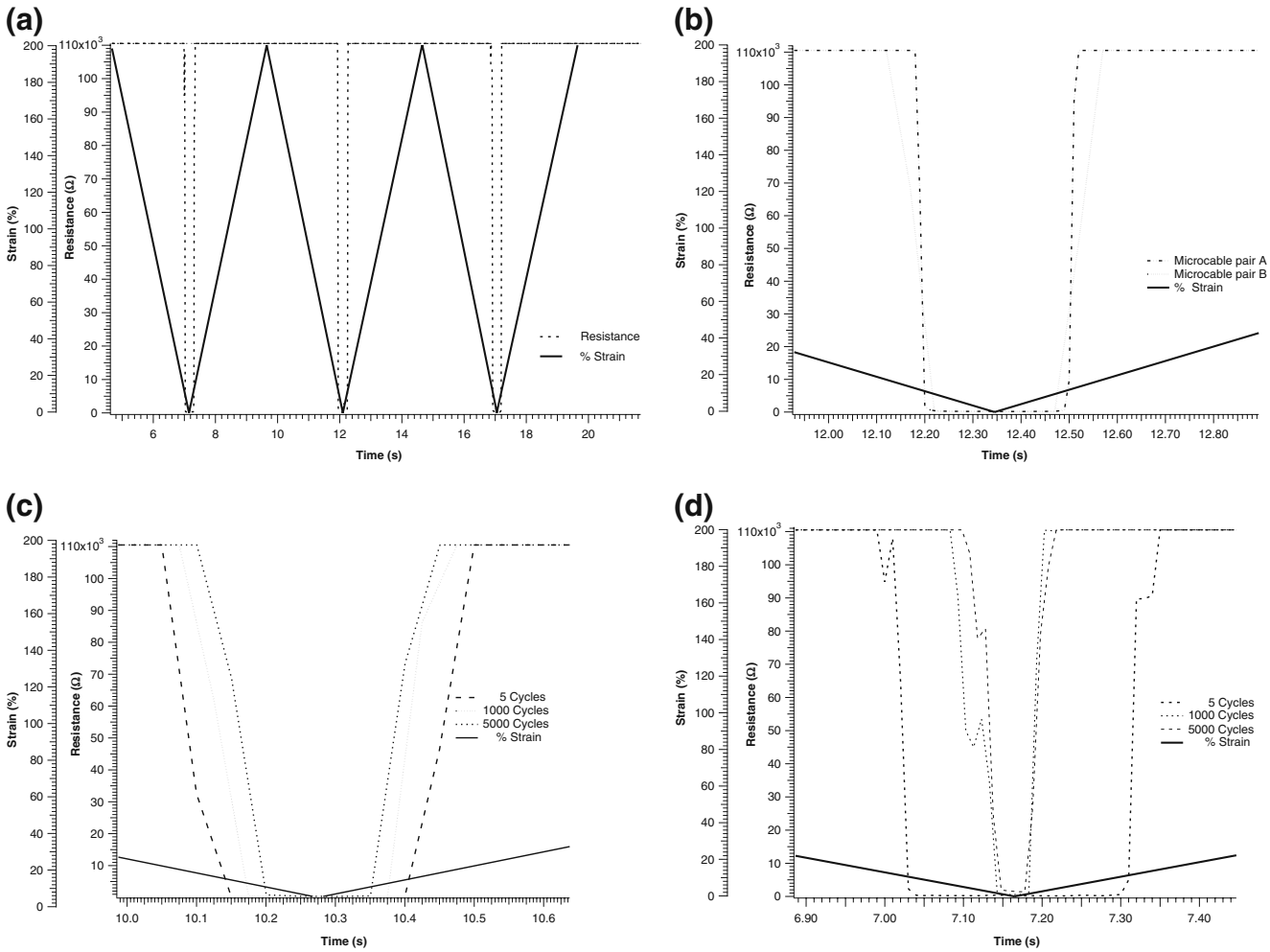

Fig. 5 (**a**) The electromechanical response to 200% applied strain is shown above over multiple cycles with the corresponding strain profile. The strain rate is 80% per second (absolute displacement: 1.92 mm/s, 4.8 mm per 5 s, 0.2 Hz. (**b**) An expanded view after five cycles of strain is shown with the resistance profile of two sets of microcables overlaid for reference. The two samples tested had a measurable conductivity to 7 & 9% strain, respectively. (**c-d**) The full test, measuring resistance after 1,000 and 5,000 cycles, for each microcable pair is shown

4.4 Electrophysiological measurements

The array of two microcables was threaded around the sciatic nerve with a pair of forceps (Fig. 6(b)-(c)) similar to the electrodes wrapped around the nerve in Fig. 1. An additional single microcable was threaded around the nerve approximately 1 cm distal from the double electrode array (Fig. 6(b)-(c)). The electrophysiological recordings are shown in Fig. 6(a)-(c). Control recordings were measured with a pair of uninsulated stainless steel wire electrodes 2 mm apart (wire diameter: 0.5 mm; cross-sectional area: 0.19 mm^2 vs. 0.017 mm^2 for microcable electrodes). The sharp initial peak is the stimulus artifact, while the differentially recorded compound action potential is visible several milliseconds afterward. The two differential recordings from the microcable electrodes are shown in Fig. 6(b)-(c). The differential recording in Fig. 6(b)-(c) was obtained from the microcable-pair array, with a recording site separation of 1 mm. The recording in Fig. 6(c) shows the differential amplitude between one of the electrodes in the pair array and the third microcable, with a recording separation of 1 cm.

5 Discussion

The microcable electrodes were designed to function in electrophysiological applications with irregular or highly-curved surfaces that require a small footprint. The compliance and elasticity of the microcable electrode necessitates benchmarking the mechanical properties to identify functional parameters. The microcable substrate cross-section was minimized by using a mix of Sylgard 184/186, rather than using Sylgard 184, which improved the ultimate

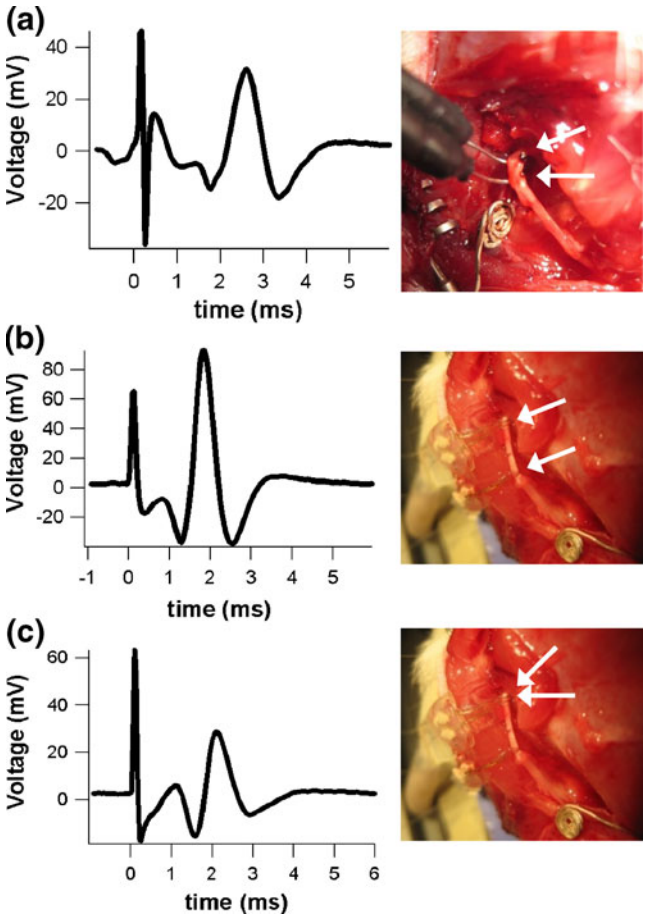

Fig. 6 The differential recording is shown (**a**) between a pair of hook electrodes spaced 2 mm apart, (**b**) between a pair of microcables spaced 1 cm apart and (**c**) between a pair of attached microcables (1 mm apart). In (**b**) and (**c**) the microcable arrays are in close contact with the nerve, conforming around its circumference. The electrodes were threaded under the nerve and pulled through to the other side with tweezers for positioning. The recording demonstrates that the electrodes can be curled around a small anatomical feature and obtain a successful recording. For reference, the circular ground wire is 7 mm in diameter

tensile strength by a factor of two. The modulus did increase with the addition of the gold film, but the theoretical bending stiffness, calculated as a function of cross-sectional area, was several order of magnitude less than the calculations approximating similar electrodes composed of polyimide or silicon (Table 4). The electrophysiological testing shows that the electrodes can be wrapped around small features such as a peripheral nerve for recording electrical activity.

5.1 Mechanical testing

The tensile strain test was used to characterize the PDMS substrate because it is the expected method of deformation in the mechanical handling of the microcable electrodes. The strain rate of 7–10% s^{-1} was selected because it fell within the range of anticipated strain rates during handling. The Young's modulus of the Sylgard 184/186 mix was not statistically different from the modulus of the Sylgard 184 (Table 2), showing that the strength of the substrate could be increased without compromising a low-Young's modulus. The mechanical substrate may be further optimized by reducing the cross-linking density of the PDMS substrate. The reduction in the substrate modulus would also likely reduce the conductivity of the gold film under applied strain as the literature shows a correlation between the Young's modulus of the substrate and the minimization of strain localization in the metal film (Li and Suo 2006). The modulus of Sylgard 186 structures, which were not evaluated independently due to the uneven surface of the spun-cast 186 films, have a literature reported modulus of 700–750 kPa (Bergbreiter et al. 2006; Pelrine et al. 2000). Previous reports of the Young's modulus of Sylgard 184 range from 0.4 MPA to 3 MPa (Engel et al. 2005; Schneider et al. 2008; She and Chaudhury 2000). The experimentally obtained value of 0.72 MPa for Sylgard 184 is within this range, and may be on the lower end of the reported range because of the short application of heat during processing with the remainder of curing occurring at room temperature (Schneider et al. 2008).

After 10% strain, the Young's modulus of the microcable array was 1.81 MPa, which is increased from 0.69 MPa of the microcable without the metal film. Eventhough the 30 nm thickness of the gold is less than one thousandth the thickness of the substrate, this increase is expected because gold has a modulus of 55 GPa, approximately four orders of magnitude greater than the modulus of the PDMS substrate (0.69 MPa). Given the difference in the materials' Young's moduli, the approximately three-fold increase in the composite moduli, at 1.8 MPa, is still lower than the the moduli of other substrates (Table 1). Because the layer of metal was very thin, and cracked, its increase in the composite Young's modulus is lower (Begley and Bart-Smith 2005). As the crack density increases under the higher strains (40%), the modulus decreases by about 10% to 1.62 MPa. This decrease agrees with the theory previously described in the literature, although the mathematical relations describing the relation between crack density and modulus are approximate (Begley and Bart-Smith 2005). The cracks also may reduce residual stress in the film (Ye et al. 1992). Stress accumulation might be cause for concern in a device intended to be highly compliant and conformal; however, because of the low substrate modulus, the any stress accumulation appears to be concentrated in the gold film, visible by the wrinkles in the metal.

The experimentally obtained Young's modulus of the microcable electrodes was used to calculate the theoretical bending stiffness using an analytical model. The experi-

mental modulus accounts for the reduced stiffness in the gold film due to strain-induced cracks, while the bilayer beam model does not. This difference is expected to contribute to the discrepancy in the calculations: $1.9*10^{-11}$ vs $2.7*10^{-11}$ MPa $\cdot m^4$. Additionally, the modulus for gold was taken from the literature and the effective value for the 30 nm gold film may be different due to the stress induced from the mismatch in thermal expansion coefficients, crystallinity and thin-film related phenomena (Bowden et al. 1998; Qi et al. 2003; Van Swygenhoven and Weertman 2006).

The theoretical bending stiffness is an order of magnitude lower than the estimated value for a polyimide electrode, and two orders of magnitude lower than that for a silicon electrode. This suggests that the compliant microcable electrodes might elicit a reduced inflammatory relative to that of the conventionally used silicon electrodes when used as cortical implants. This trend has already been demonstrated with parylene electrodes that have a ladder like-architecture to reduce the bending stiffness (Seymour and Kipke 2007). The difficulty in using highly-compliant electrodes for intracortical applications is the availability of an accompanying effective and reliable insertion technique. The composite modulus is still stiffer than that of the brain (690 kPa vs. 3.5 kPa (Green et al. 2008)) but is not stiff enough to insert without the addition of a guiding shuttle or a degradable coating. Examples of these strategies have been successfully demonstrated. Functionalized shuttles with water-activated coatings are able to both deploy and release PDMS structures with shank-style electrode geometries (Jaroch et al. 2009; Kozai and Kipke 2009). Alternatively, biodegradable coatings to ease insertion could also be used (Paralikar and Clement 2008).

5.2 Electromechanical response to strain

The application of strain to the microcable electrodes causes elastic deformation in the PDMS substrate and plastic deformation and crack formation in the gold film. A conductive path forms in between the cracks of the gold film (Lacour et al. 2006). The stability of this path at low numbers of relatively large applications of strain suggests that the electrodes are not likely to suffer damage either during acute use or during implantation procedures. The increasing baseline resistance with increasing strain cycles suggests a lack of reconnection at low strains between the conductive islands, either due to wear at the island interfaces or to creep in the substrate from the cyclic application of stretch. The increase in the percent standard deviation with each of the measurements may be due to an increase in the potential number of connective paths from the increased crack density or, possibly, the presence of delaminated particles from the metal film which move and alter the path of conductivity with each strain.

The stretch tests were designed to determine if the microcable electrodes could be tugged or pulled into position during placement. As such, the strain was applied along the long axis of the microcables. The electrodes may also be expected to encounter strain across the width of the microcable from compressive forces if the electrode is pinched or otherwise pinned along its length; however, assuming the gold film and PDMS are isotropic along the length and width of the electrode, simple cases of this scenario can be calculated from the strain tests on the long axis of the microcables. The 200% strain was chosen because it was safely below the failure strain of the Sylgard 184/186 mix. As demonstrated, the conductivity is preserved after the strain is released, even after 1,000 and 5,000 cycles, although range of strain for low resistance is shown to reduce. The resistance profile was measured up to 220 kΩ because of instrumentation limitations, but higher measurements are of limited use because the resistance is greater than the impedance value of the electrode site, 100 kΩ (at 1 kHz). Relatively small resistance changes do little to change the electrode recording capability. When the resistance increase becomes large enough to change the impedance value of the electrode, it interferes with the electrode function.

The reduction in the strain with measureable resistance after 1,000 & 5,000 cycles was not investigated but may be due to wear in the gold film, although stress-relaxation in the PDMS substrate may have also contributed (Smith 1993). The rate of resistance increase was different in the two samples tested. This may be due to intrinsic sample variation but might be improved by optimizing and refining the consistency of the deposition parameters for the thin-film gold. Elastomeric microelectrodes have been presented previously and shown conductivity up to 30% strain, although device performance at much higher strains (i.e. 200%) was not described (Graz et al. 2009; Lacour et al. 2006; Yu et al. 2006). We have not been able to replicate the same strain-conductivity relation at 30% strain. There were some variations between the two devices that may have contributed to this difference. The deposition method for the devices conductive at 30% stain was E-beam evaporation (Graz et al. 2009; Lacour et al. 2005, 2006; Yu et al. 2006) while the microcable electrodes were patterned with thermal evaporation. The radiation from the E-beam deposition may have increased the modulus of the substrate at the surface, improving the capacity of the substrate to dissipate localized strain (Li and Suo 2006). Alternately, the Young's modulus of the Sylgard 184/186 is 0.69 MPa, while the value of the PDMS substrate used for the 30% strain conductivity measurements may have been higher. There are a number of other variables such as the

deposition rate or the applied strain rate that could have contributed to this difference. We did not investigate the discrepancy further because the electromechanical testing of the microcables showed that they could be stretched for acute use scenarios without failure. Under small strains, the resistance of the film may fluctuate over a few hundred ohms, but the change is small relative to the impedance at the recording site, suggesting that it will not hinder the electrical functionality. The strain-free conductivity is less than 1% of the impedance of the recording site (<400Ω vs.100 kΩ). Situating the electrode under tension in a chronic implant or even in an acute setting during electrophysiological testing is likely inadvisable because of the stress that would be transferred to the tissue. In electrode design, avoiding tensile loading and strain in the electrode is generally avoided in the design to the extent possible (Kumar et al. 2006; Scheiner et al. 1994). The strain-tolerant multi-electrode membrane described by Graudejus et al. was designed for use with a stretch injury protocol, which is a rather specialized electrophysiological application (Graudejus et al. 2009). It is possible that the microcables could be optimized for the strain-conductivity described by Graudejus et al. if the variables of the deposition, substrate and strain testing were studied in a systematic manner.

5.3 Electrophysiological testing

The differential recording of the evoked compound action potential demonstrates the recording capability of the microcable electrodes. The signal from the microcable electrodes is comparable to the signal measured with the standard stainless steel hook electrodes. Although direct comparisons between the microcable and control electrodes cannot be made, the characteristic shape of a compound action potential is visible in all recordings.

The impedance of the large control electrodes is minimal because the wires were uninsulated, while the impedance for the microcable electrodes was 100 kΩ (at 1 kHz) as measured with an impedance conditioning module (ICM neuro/craft; FHC Inc, Bowdoin, ME).

The integrity of the microcable electrodes under chronic implant conditions has not yet been tested, however the literature suggests the devices are suitable for the *in vivo* environment or could be made so with design modifications to maximize the integrity of the insulating layers (Anderson et al. 1988; Morent et al. 2007; von Metzen and Stieglitz 2007). Multi-electrode arrays fabricated from thin-film gold and PDMS have been successfully used in culture-wells for organotypic brain slices over 12 days (Yu et al. 2009). The time-span, while shorter than that of a chronic implant, is still a pertinent data point in the assessment of PDMS and thin-film gold electrode durability and functionality. The recording site would likely be modified on an application-by-application basis, as the area of electrode surface optimization is a complex research and clinical issue (Cogan 2008).

6 Conclusion

Microcable electrodes have been fabricated with the common techniques of photolithography and spin-casting to make the process accessible to general implementation. The resulting electrodes were shown to demonstrate mechanical durability and electrophysiological functionality. The microcable array profile allows for the electrodes to be wrapped around small features such as the peripheral nerve and for variable placement. The mechanics of thin-film metal on a compliant substrate allow the gold to crack in numerous places without a permanent loss of electrical continuity after the strain is released. A low Young's modulus was achievable because of the thin, cracked morphology of the gold film and the low-modulus PDMS substrate. Based on the data in the literature, it may be possible to further improve the quality of the film so that the electrical continuity is preserved at an strain greater than 8%. The microcable electrode mechanical properties warrant further study as a chronic implant to determine the response of the tissue relative to other electrodes. If the microcable electrodes were to be used in a chronic study, it is conceivable from the compliance that they could be wrapped around the nerve and sutured into a cuff formation or inserted as a shank-style array with a shuttle or biodegradable coating.

References

T. Adrega, Lacour, S.P., Stretchable gold conductors embedded in PDMS and patterned by photolithography: fabrication and electromechanical characterization. J. Micromech. Microeng. **20** (5) (2010).

A.T. Al-Halhouji, I. Kampen, T. Krah, S. Buttgenbach, Nanoindentation testing of SU-8 photoresist mechanical propterties. Microelectron. Eng. **85**(5–6), 942–944 (2008)

J.E. Anderson, V. Markovac, P.R. Troyk, Polymer encapsulants for microelectronics—mechanisms for protection and failure. IEEE Trans. Components. Hybrids. Manuf. Technol. **11**(1), 152–158 (1988)

M.R. Begley, H. Bart-Smith, The electro-mechanical response of highly compliant substrates and thin stiff films with periodic cracks. Int. J. Solids Struct. **42**(18–19), 5259–5273 (2005)

S. Bergbreiter, Elastomer-based micromechanical energy storage system, *In IMECE* (2006).

R. Biran, Martin, D.C., & Tresco, P.A., The brain tissue response to implanted silicon microelectrode arrays is increased when the device is tethered to the skull. J. Biomed. Mater. Res. Part A, 169–178, (2007)

G.H. Borschel, K.F. Kia, W.M. Kuzon, R.G. Dennis, Mechanical properties of acellular peripheral nerve. J. Surg. Res. **114**(2), 133–139 (2003)

N. Bowden, S. Brittain, A.G. Evans, J.W. Hutchinson, G.M. Whitesides, Spontaneous formation of ordered structures in thin films of metals supported on an elastomeric polymer. Nature **393**(6681), 146–149 (1998)

V. Chiono, G. Vozzi, F. Vozzi, C. Salvadori, F. Dini, F. Carlucci, M. Arispici, S. Burchielli, F. Di Scipio, S. Geuna, M. Fornaro, P. Tos, S. Nicolino, C. Audisio, I. Perroteau, A. Chiaravalloti, C. Domenici, P. Giusti, G. Ciardelli, Melt-extruded guides for peripheral nerve regeneration. Part I: poly(epsilon-caprolactone). Biomed. Microdevices **11**(5), 1037–1050 (2009)

I.P. Clements, Y.T. Kim, A.W. English, X. Lu, A. Chung, R.V. Bellamkonda, Thin-film enhanced nerve guidance channels for peripheral nerve repair. Biomaterials **30**(23–24), 3834–3846 (2009)

S.F. Cogan, Neural stimulation and recording electrodes. Annu. Rev. Biomed. Eng. **10**, 275–309 (2008)

DuPont. DuPont flexible substrates for thin film BIPV and concentrate PV. 1-2. (2009).

Engel, J.M., Chen, J., Bullen, D., & Liu, C. Polyurethane rubber as a mems material: Characterization and demonstration of an all-polymer two-axis artificial hair cell flow sensor. *MEMS 2005 Miami: Technical Digest*, 279–282. (2005)

J. Garra, T. Long, J. Currie, T. Schneider, R. White, M. Paranjape, Dry etching of polydimethylsiloxane for microfluidic systems. J. Vacuum Sci. Technol. A Vacuum Surf. Films **20**(3), 975–982 (2002)

V.M. Graubner, R. Jordan, O. Nuyken, T. Lippert, M. Hauer, B. Schnyder, A. Wokaun, Incubation and ablation behavior of poly (dimethylsiloxane) for 266 nm irradiation. Appl. Surf. Sci. **197**, 786–790 (2002)

O. Graudejus, Z. Yu, J. Jones, B. Morrison, S. Wagner, Characterization and application of an elastically stretchable microelectrode array to neural field potential recordings. J. Electrochem. Soc. **156**(6), P85–P94 (2009)

I.M. Graz, Cotton, D.P.J., & Lacour, S.P., Extended cyclic uniaxial loading of stretchable gold thin-films on elastomeric substrates. Appl. Phys. Lett. **94** (7) (2009)

M.A. Green, L.E. Bilston, R. Sinkus, *In vivo* brain viscoelastic properties measured by magnetic resonance elastography. NMR Biomed. **21**(7), 755–764 (2008)

J.R. Greer, W.C. Oliver, W.D. Nix, Size dependence in mechanical properties of gold at the micron scale in the absence of strain gradients (vol 53, pg 1821, 2005). Acta Mater. **54**(6), 1705 (2006)

W. He, R. Bellamkonda, *A molecular perspective on understanding and modulating the performance of chronic central nervous system recording electrodes. In A molecular perspective on understanding and modulating the performance of chronic central nervous system recording electrodes* (CRC, Boca Raton, 2008)

N. Jackson, S. Anand, M. Okandan, J. Muthuswamy, Nonhermetic encapsulation materials for MEMS-based movable microelectrodes for long-term implantation in the brain. J. Microelectromech. Syst. **18**(6), 1234–1245 (2009)

D.B. Jaroch, M.P. Ward, E.Y. Chow, J.L. Rickus, P.P. Irazoqui, Magnetic insertion system for flexible electrode implantation. J. Neurosci. Meth. **183**(2), 213–222 (2009)

T.D.Y. Kozai, D.R. Kipke, Insertion shuttle with carboxyl terminated self-assembled monolayer coatings for implanting flexible polymer neural probes in the brain. J. Neurosci. Meth. **184**(2), 199–205 (2009)

K. Kumar, J. Wilson, R. Taylor, S. Gupta, Complications of spinal cord stimulation, suggestions to improve outcome, and financial impact. J. Neurosurg. Spine **5**(9), 191–203 (2006)

S.P. Lacour, Chan, D., Wagner, S., Li, T., & Suo, Z.G., Mechanisms of reversible stretchability of thin metal films on elastomeric substrates. Appl. Phys. Lett. **88**(20) (2006)

S.P. Lacour, J. Jones, Z. Suo, S. Wagner, Design and performance of thin metal film interconnects for skin-like electronic circuits. IEEE Electron Device Lett. **25**(4), 179–181 (2004)

S.P. Lacour, C. Tsay, S. Wagner, Z. Yu, B. Morrison, Stretchable micro-electrode arrays for dynamic neuronal recording of *in vitro* mechanically injured brain. Ieee Sens **1 and 2**, 617–620 (2005)

T. Li, Z. Suo, Deformability of thin metal films on elastomer substrates. Int. J. Solids Struct. **43**(7–8), 2351–2363 (2006)

M. Maiti, M. Bhattacharya, A.K. Bhowmick, Elastomer nanocomposites. Rubber Chem. Technol. **81**(3), 384–469 (2008)

J.E. Mark, Some novel polymeric nanocomposites. Acc. Chem. Res. **39**(12), 881–888 (2006)

M.A. McClain, LaPlaca, M.C., & Allen, M.G., Spun-cast micromolding for etchless micropatterning of electrically functional PDMS structures. J. Micromech. Microeng. **19**(10) (2009)

K.W. Meacham, R.J. Giuly, L. Guo, S. Hochman, S.P. DeWeerth, A lithographically-patterned, elastic multi-electrode array for surface stimulation of the spinal cord. Biomed. Microdevices **10**(2), 259–269 (2008)

R. Morent, N. De Geyter, F. Axisa, N. De Smet, L. Gengembre, E. De Leersnyder, C. Leys, J. Vanfleteren, M. Rymarczyk-Machal, E. Schacht, E. Payen, Adhesion enhancement by a dielectric barrier discharge of PDMS used for flexible and stretchable electronics. J. Phys. D Appl. Phys. **40**(23), 7392–7401 (2007)

Y. Nam, K. Musick, B.C. Wheeler, Application of a PDMS microstencil as a replaceable insulator toward a single-use planar microelectrode array. Biomed. Microdevices **8**(4), 375–381 (2006)

E. Ostuni, R. Kane, C.S. Chen, D.E. Ingber, G.M. Whitesides, Patterning mammalian cells using elastomeric membranes. Langmuir **16**(20), 7811–7819 (2000)

K.J. Paralikar, R.S. Clement, Collagenase-aided intracortical microelectrode array insertion: effects on insertion force and recording performance. IEEE Trans. Biomed. Eng. **55**(9), 2258–2267 (2008)

R. Pelrine, R. Kornbluh, J. Joseph, R. Heydt, Q.B. Pei, S. Chiba, High-field deformation of elastomeric dielectrics for actuators. Mater. Sci. Eng. C Biomimetic Supramol. Syst. **11**(2), 89–100 (2000)

Pornsin-Sirirak, T.N., Tai, Y.C., Nassef, H., & Ho, C.M. 2001. *Flexible parylene actuator for micro adaptive flow control*.

H.J. Qi, K. Joyce, M.C. Boyce, Durometer hardness and the stress-strain behavior of elastomeric materials. Rubber Chem. Technol. **76**(2), 419–435 (2003)

S. Rosset, M. Niklaus, P. Dubois, H.R. Shea, Metal ion implantation for the fabrication of stretchable electrodes on elastomers. Adv. Funct. Mater. **19**(3), 470–478 (2009)

P.J. Rousche, D.S. Pellinen, D.P. Pivin, J.C. Williams, R.J. Vetter, D. R. Kipke, Flexible polyimide-based intracortical electrode arrays with bioactive capability. IEEE Trans. Biomed. Eng. **48**(3), 361–371 (2001)

A. Sayah, V.K. Parashar, M.A.M. Gijs, LF55GN photosensitive flexopolymer: a new material for ultrathick and high-aspect-ratio MEMS fabrication. J. Microelectromech. Syst. **16**(3), 564–570 (2007)

A. Scheiner, G. Polando, E.B. Marsolais, Design and clinical application of a double helix electrode for functional electrical stimulation. IEEE Trans. Biomed. Eng. **41**(5), 425–431 (1994)

F. Schneider, Fellner, T., Wilde, J., & Wallrabe, U., Mechanical properties of silicones for MEMS. J. Micromech. Microeng. **18**(6) (2008)

J.P. Seymour, D.R. Kipke, Neural probe design for reduced tissue encapsulation in CNS. Biomaterials **28**(25), 3594–3607 (2007)

H.Q. She, M.K. Chaudhury, Estimation of adhesion hysteresis using rolling contact mechanics. Langmuir **16**(2), 622–625 (2000)

S.K. Sia, G.M. Whitesides, Microfluidic devices fabricated in poly (dimethylsiloxane) for biological studies. Electrophoresis **24**(21), 3563–3576 (2003)

L. Smith, *The language of rubber* (Butterworth-Heinemann, Oxford, 1993)

T. Someya, T. Sekitani, S. Iba, Y. Kato, H. Kawaguchi, T. Sakurai, A large-area, flexible pressure sensor matrix with organic field-effect transistors for artificial skin applications. Proc. Natl Acad. Sci. USA **101**(27), 9966–9970 (2004)

P. Stice, A. Gilletti, A. Panitch, J. Muthuswamy, Thin microelectrodes reduce GFAP expression in the implant site in rodent somatosensory cortex. J. Neural Eng. **4**, 42–53 (2007)

J.M. Subbaroyan, D.R. Kipke, A finite-element model of the mechanical effects of implantable microelectrodes in the cerebral cortex. J. Neural Eng. **2**(4), 10 (2005)

Y.J. Sun, B. Akhremitchev, G.C. Walker, Using the adhesive interaction between atomic force microscopy tips and polymer surfaces to measure the elastic modulus of compliant samples. Langmuir **20**(14), 5837–5845 (2004)

K. Takei, T. Kawashima, T. Kawano, H. Kaneko, K. Sawada, M. Ishida, Out-of-plane microtube arrays for drug delivery-liquid flow properties and an application to the nerve block test. Biomed. Microdevices **11**(3), 539–545 (2009)

H. Van Swygenhoven, J.R. Weertman, Deformation in nanocrystalline metals. Mater. Today **9**(5), 24–31 (2006)

R.P. von Metzen, T. Stieglitz, A wireless system for monitoring polymer encapsulations. 2007 Annu. Int. Conf. Ieee Eng. Med. Biol. Soc. **1–16**, 6601–6604 (2007)

J.M. Wasikiewicz, N. Roohpour, D. Paul, M. Grahn, D. Ateh, I. Rehman, P. Vadgama, Polymeric barrier membranes for device packaging, diffusive control and biocompatibility. Appl. Surf. Sci. **255**(2), 340–343 (2008)

R. Weast, *Handbook of chemistry and physics*, 60th edn. (CRC, Boca Raton, 1979)

D.F. Williams, On the mechanisms of biocompatibility. Biomaterials **29**(20), 2941–2953 (2008)

C.P. Wu, W.P. Luk, J. Gillis, F. Skinner, L. Zhang, Size does matter: generation of intrinsic network rhythms in thick mouse hippocampal slices. J. Neurophysiol. **93**(4), 2302–2317 (2005)

Y.N. Xia, G.M. Whitesides, Soft lithography. Annu. Rev. Mater. Sci. **28**, 153–184 (1998)

T. Ye, Z. Suo, A. Evans, Thin film cracking and the roles of substrate and interface. Int. J. Solids Struct. **29**(21), 2639–2648 (1992)

W.C. Young, *Roark's formulas for stress and strain*, 6th edn. (McGraw-Hill, New York, 1989)

Z. Yu, O. Graudejus, C. Tsay, S.P. Lacour, S. Wagner, B. Morrison, Monitoring electrical activity from hippocampal tissue during large electrode deformation. J. Neurotrauma **26**, 1135–1145 (2009)

Yu, Z., Tsay, C., Lacour, S.P., Wagner, S., & Morrison, B. 2006. Stretchable microelectrode arrays- a tool for discovering mechanisms of functional deficits underlying traumatic brain injury and interfacing neurons with neuroprosthetics. *Conf Proc IEEE Eng Med Biol Soc Suppl*, 6732–6735.

Z. Yu, O. Graudejus, C. Tsay, S.P. Lacour, S. Wagner, B. Morrison, A new tool for monitoring neuroelectrical activity during brain tissue deformation: stretchable microelectrode arrays. J. Neurotrauma **24**(7), 200 (2007)